

Visual Privacy Auditing with Diffusion Models

Kristian Schwethelm¹, Johannes Kaiser¹, Moritz Knolle¹, Daniel Rückert^{1,2}, Georgios Kaissis^{*1,2,3},
and Alexander Ziller^{*1}

¹Chair for Artificial Intelligence in Medicine, Technical University of Munich, Germany

²Department of Computing, Imperial College London, United Kingdom

³Institute for Machine Learning in Biomedical Imaging, Helmholtz Munich, Germany

Abstract

Image reconstruction attacks on machine learning models pose a significant risk to privacy by potentially leaking sensitive information. Although defending against such attacks using differential privacy (DP) has proven effective, determining appropriate DP parameters remains challenging. Current formal guarantees on data reconstruction success suffer from overly theoretical assumptions regarding adversary knowledge about the target data, particularly in the image domain. In this work, we empirically investigate this discrepancy and find that the practicality of these assumptions strongly depends on the domain shift between the data prior and the reconstruction target. We propose a reconstruction attack based on diffusion models (DMs) that assumes adversary access to real-world image priors and assess its implications on privacy leakage under DP-SGD. We show that (1) real-world data priors significantly influence reconstruction success, (2) current reconstruction bounds do not model the risk posed by data priors well, and (3) DMs can serve as effective auditing tools for visualizing privacy leakage.

1 Introduction

In an era characterized by the collection of vast image datasets containing sensitive information like personal identities, private locations, or medical conditions, the question of safeguarding individual privacy becomes paramount. Within the domain of machine learning (ML), the effectiveness of models heavily relies on the data they are trained with. Nevertheless, ML models are known for their potential to leak private information from their training data [6, 18, 20, 21].

This growing privacy concern has drawn considerable attention to developing privacy-preserving techniques for ML tasks. Among these, differential privacy (DP) [15] has emerged as the gold standard for providing formal pri-

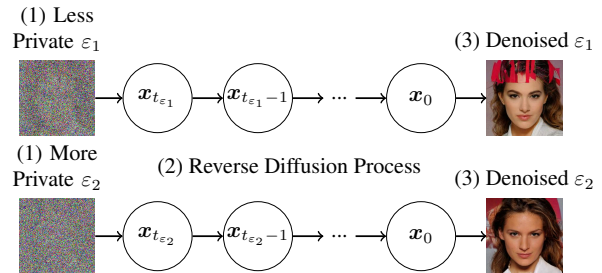


Fig. 1: (1) Our reconstruction attack first extracts a noisy image from a DP algorithm with privacy guarantee ϵ_n [4, 56]. (2) Then, it employs a DM for denoising by initiating its reverse diffusion process from an intermediate state $x_{t_{\epsilon_n}}$ with a matching noise variance. (3) We demonstrate DMs’ strong denoising capabilities and utility for visual auditing, aiding communication with non-experts. For instance, it is possible to infer that ϵ_1 offers little privacy protection, allowing accurate reconstruction, while ϵ_2 safeguards certain details but still allows disclosure of high-level personal attributes.

vacuity guarantees. However, the extent to which DP defends against real-world privacy attacks, particularly in data reconstruction scenarios where adversaries attempt to reconstruct complete individual data records, remains uncertain. This uncertainty is concerning, given that practitioners face privacy-utility trade-offs, where stronger privacy guarantees often entail performance losses. Thus, practitioners seeking to minimize the impact of privacy techniques must understand how well weaker privacy guarantees safeguard sensitive information.

Attempts to address this issue have led to the development of formal upper bounds on data reconstruction success under DP, aiming to enable practitioners to assess the effect of DP guarantees on the maximum fidelity achievable by an adversary’s reconstruction attack. Central to such bounds are the formalized threat models, which define the capabilities of potential adversaries and the scenarios under which the bounds hold. Due to the complexity of mathematically formalizing practical scenarios, overly pessimistic threat models that account for the most

*Equal contribution.

powerful (worst-case) attacks have been adopted [2, 19]. Although these bounds offer generality and hold against all possible attacks, they usually overestimate the threat in real-world scenarios [55]. For instance, while Hayes *et al.* [21] demonstrate the near-tightness of the reconstruction robustness (ReRo) bound [2], these bounds still assume a highly informed adversary with access to a prior distribution that includes the target record.

As a result, there is an ongoing effort to formulate practical reconstruction bounds tailored to realistic attack scenarios. Ziller *et al.* [56] derive formal bounds on error measures for a specific reconstruction attack on DP training, assuming an uninformed adversary capable of selecting model architecture and hyperparameters but lacking prior knowledge about the data. Their threat model, however, is overly optimistic in scenarios where data priors are common, particularly in the image domain, where the underlying data structure and characteristics are well known. The missing consideration for realistic data priors represents a significant gap in the current analyses of data reconstruction attacks under DP.

In this work, we address this gap and empirically investigate the effect of DP on defending against image reconstruction attacks leveraging real-world data priors. We compare our findings with the guarantees given by the (worst-case) ReRo [21] and Ziller *et al.*'s [56] bounds. To ensure comparability with the aforementioned works, we adopt the threat model and reconstruction attack of Ziller *et al.* and incorporate image priors approximating the underlying data distribution of the reconstruction target. Building upon the observation that their attack is equivalent to attempting to reconstruct an image perturbed with additive noise [4], we propose an extension that leverages strong image priors learned by diffusion models (DMs) [12, 23] to denoise the reconstructions (see Fig. 1). This enables us to model adversarial access to real-world data priors.

Our findings reveal the significant influence of data priors on reconstruction success, with their impact varying depending on the strength of the prior (inherent distribution shift). Currently, no works assessing reconstruction bounds model these considerations. Instead, they rely on simplified assumptions not applicable in real-world scenarios. Additionally, our approach allows even stakeholders without technical experience to visually audit the protection against reconstruction attacks. Overall, our study sheds light on the shortcomings of current reconstruction bounds and contributes to a better understanding of the practical implications of DP in real-world scenarios.

Our main contributions can be summarized as follows:

1. We propose an image reconstruction attack based on DMs to model adversary access to realistic data priors. We demonstrate the significant threat such priors pose in disclosing private information under DP.

2. We show that realistic reconstruction success strongly depends on the strength of the data prior, which is not modeled well by any theoretical bound.
3. We empirically identify privacy parameters necessary to defend against our attack and demonstrate its efficacy as a visual auditing tool.

2 Related Works

Understanding DP Guarantees. DP guarantees that the probability of an algorithm's output being correctly assigned to its input is upper bounded. Typically, this guarantee is quantified using parameters such as ϵ and δ to measure the level of privacy preservation of an algorithm. However, a more operationally interpretable way of quantifying privacy is by attributing practical risk against certain attacks under specific threat models. Thus, many works try to shed light on the practical effects of DP by investigating, *e.g.*, auditing [31, 32, 44], relaxed threat models [33, 55], privacy attacks [5, 18, 53], and deployment [9, 36]. However, to the best of our knowledge, the effect of real-world data priors remains underexplored. In this work, we leverage image priors learned by diffusion models to gain deeper insights into privacy leakage under practical reconstruction attacks.

While there is considerable exploration of theoretical [13, 26] and empirical [33] bounds for membership inference attacks, formalizing the threat posed by reconstruction attacks that aim to disclose the training data remains challenging, especially in realistic scenarios [55]. Thus, we identify a requirement for works like ours, which express real-world privacy risks and assist practitioners in navigating privacy-utility trade-offs.

Image Denoising. Image denoising is a classic ill-posed problem in image processing, where early successes with filtering-based methods [7, 10] evolved into remarkable successes with deep learning methods [16]. Recently, generative image denoising strategies leveraging diffusion models have demonstrated state-of-the-art perceptual quality in natural [35, 50, 51] and medical imaging [8, 48, 49]. Notably, in the broader field of image restoration, diffusion models have also demonstrated significant efficacy in tasks like super-resolution, colorization, and inpainting [30].

In contrast to these works, we do not aim to enhance image quality by removing some minor natural noise. Instead, we aim to recover private information from deliberately perturbed images with substantial noise scales introduced to provide DP guarantees.

3 Background

This section briefly introduces the fundamental concepts our work builds upon, *i.e.*, differential privacy and diffusion models.

3.1 Differential Privacy Guarantees

Differential privacy (DP) [15] is a formal guarantee that provably bounds privacy leakage from computations on datasets.

Definition 1. A randomized algorithm (mechanism) \mathcal{M} satisfies (ϵ, δ) -DP if, for any pairs of adjacent datasets $D \simeq D'$ that differ in a single sample and all sets of outcomes $\mathcal{S} \subseteq \text{Range}(\mathcal{M})$, it holds that:

$$\Pr[\mathcal{M}(D) \in \mathcal{S}] \leq e^\epsilon \Pr[\mathcal{M}(D') \in \mathcal{S}] + \delta. \quad (1)$$

Intuitively, DP limits the influence of an individual sample on the algorithm’s outcome. In this work, we focus on the Gaussian mechanism (GM), a standard DP mechanism often used in ML. GMs introduce controlled randomization to mask the contribution of a sample through the addition of i.i.d. Gaussian noise $\mathcal{N}(0, \Delta_2^2 \sigma^2 \mathbf{I})$, where the variance of the noise is calibrated to the privacy guarantee using noise multiplier σ and the mechanism’s global L_2 -sensitivity Δ_2 [3].

The standard threat model to analyze the privacy risk under DP is very pessimistic, assuming an adversary with complete knowledge, except for the noise realization and whether D or D' was used to compute the mechanism’s outcome. The latter aspect naturally aligns DP with membership inference attacks, which aim to determine whether a specific individual’s data was part of the dataset [52].

The prevailing approach to implementing DP in ML is DP-Stochastic Gradient Descent (DP-SGD) [1, 42], which limits the privacy leakage from neural network training. DP-SGD is a modified version of SGD that enforces an upper bound on sensitivity $\Delta_2 = C$ by clipping per-sample gradients to an upper norm bound C and adding calibrated i.i.d. Gaussian noise $\mathcal{N}(0, C^2 \sigma^2 \mathbf{I})$.

Reconstruction Robustness (ReRo) [2, 21, 25]. ReRo is a formal upper bound on the probability of a successful data reconstruction attack.

Definition 2. A randomized algorithm (mechanism) \mathcal{M} satisfies (η, γ) -ReRo if, for any reconstruction attack R on the algorithm’s outcome ω , any dataset $D_- \cup \{z\}$, where z denotes the reconstruction target sampled from prior π , fixed error function ρ , and baseline success probability $\kappa_{\pi, \rho}(\eta)$, it holds that:

$$\kappa_{\pi, \rho}(\eta) \leq \mathbb{P}_{z \sim \pi, \omega \sim \mathcal{M}(D_- \cup \{z\})}(\rho(z, R(\omega)) \leq \eta) \leq \gamma. \quad (2)$$

ReRo adopts the DP threat model with the slight modification that only a fixed part of the dataset D_- is known to the adversary, while the added reconstruction target z is not. However, the adversary has some prior knowledge π about the target, which, informally, serves as a reference distribution for z .

Given the difficulty in determining ρ , η , and π , as well as approximating $\kappa_{\pi, \rho}(\eta)$, Hayes *et al.* [21] introduced a worst-case ReRo definition based on sample matching, *i.e.*, $(0, \gamma)$ -ReRo. Let $\rho = \mathbb{1}(z \neq R(\omega))$, $\eta = 0$, $\kappa_{\pi, \rho}(\eta) = 1/n$, and π be a uniform distribution over a discrete set of n candidate samples $\{z_{\text{target}}, z_1, \dots, z_{n-1}\}$. Then, the adversary’s task simplifies to re-identify the target by matching the observation ω to the correct sample from the prior set.

This work utilizes $(0, \gamma)$ -ReRo as it is currently the only practical implementation of ReRo. For simplicity, we use $(0, \gamma)$ -ReRo and ReRo synonymously.

Reconstruction Bounds by Ziller *et al.* [56]. Ziller *et al.* introduced formal bounds on error metrics, including mean squared error (MSE), peak signal-to-noise-ratio (PSNR), and normalized cross-correlation (NCC) [37], for a specific data reconstruction attack on DP-SGD training. Their threat model assumes an uninformed adversary with no prior knowledge about the data but with the ability to observe gradient updates and set the model architecture and hyperparameters of the training process. Such scenarios can occur in real-world settings, *e.g.*, federated learning [4, 5, 17, 18]. With these capabilities, the adversary can configure the architecture most susceptible to privacy breaches, *i.e.*, a single fully connected layer without bias, where the output of the layer also represents the loss: $\ell = \mathbf{W}\mathbf{x}$, with \mathbf{W} denoting the weight matrix and \mathbf{x} the input data. Then, the adversary can easily invert the observed gradients and perfectly reconstruct the input using $\mathbf{x}_{\text{rec}} = \frac{\partial \ell}{\partial \mathbf{W}} = \mathbf{x}$. This shows that the input can be encoded into the gradient. However, the application of clipping and additive Gaussian noise on the gradients introduced by DP-SGD perturbs the reconstruction, leading to:

$$\mathbf{x}_{\text{rec}} = \frac{\mathbf{x}}{\max(\|\mathbf{x}\|_2/C, 1)} + \boldsymbol{\xi}, \text{ with } \boldsymbol{\xi} = \mathcal{N}(\mathbf{0}, C^2 \sigma^2 \mathbf{I}). \quad (3)$$

Leveraging the closed-form solution of this uninformed reconstruction attack, Ziller *et al.* formally analyze the reconstruction success. For example, for the mean squared error (MSE), they determine: $\text{MSE}(\mathbf{x}, \mathbf{x}_{\text{rec}}) \geq C^2 \sigma^2$.

3.2 Diffusion Models (DMs)

A standard formulation of DMs is the denoising diffusion probabilistic model (DDPM) [23], which relies on a forward diffusion process, step-wise perturbing a signal (im-

age) $\mathbf{x}_0 \sim q(\mathbf{x}_0)$ with additive i.i.d. Gaussian noise until the noise predominates. Mathematically, the forward process is described by:

$$\mathbf{x}_t = \sqrt{1 - \beta_t} \mathbf{x}_{t-1} + \sqrt{\beta_t} \boldsymbol{\epsilon}_{t-1}, \text{ with } \boldsymbol{\epsilon}_{t-1} \sim \mathcal{N}(\mathbf{0}, \mathbf{I}), \quad (4)$$

where the noise schedule $\beta_t \in (0, 1)$ controls both the variance of the noise and the factor reducing the signal at step $t = \{1, 2, \dots, T\}$. By defining $\alpha_t := 1 - \beta_t$, $\bar{\alpha}_t := \prod_{s=1}^t \alpha_s$, and given the underlying Markov chain $q(\mathbf{x}_1, \dots, \mathbf{x}_T | \mathbf{x}_0) = \prod_{t=1}^T q(\mathbf{x}_t | \mathbf{x}_{t-1})$, the noisy latent variables \mathbf{x}_t can be conditioned on \mathbf{x}_0 :

$$\mathbf{x}_t = \sqrt{\bar{\alpha}_t} \mathbf{x}_0 + \sqrt{1 - \bar{\alpha}_t} \boldsymbol{\epsilon}, \text{ with } \boldsymbol{\epsilon} \sim \mathcal{N}(\mathbf{0}, \mathbf{I}). \quad (5)$$

The core concept for generating new signals is to reverse the diffusion process using a neural network θ that approximates the intractable distribution $q(\mathbf{x}_{t-1} | \mathbf{x}_t)$ and predicts the sampled noise $\boldsymbol{\epsilon}$. Given a large number of steps T and well-behaved schedules of β_t , \mathbf{x}_T converges to a standard Gaussian. Thus, a signal can be generated by initiating the reverse process with a standard Gaussian sample and iterative denoising. The generation process is defined by:

$$\mathbf{x}_{t-1} = \underbrace{\frac{1}{\sqrt{\alpha_t}} (\mathbf{x}_t - \frac{\beta_t}{\sqrt{1 - \alpha_t}} \boldsymbol{\epsilon}_\theta(\mathbf{x}_t, t))}_{\text{Approximate } \mathbf{x}_0} + \underbrace{\sqrt{\beta_t} \boldsymbol{\epsilon}_{t-1}}_{\text{Add noise}}, \quad (6)$$

with $\boldsymbol{\epsilon}_{t-1} \sim \mathcal{N}(\mathbf{0}, \mathbf{I})$.

4 Method

In this section, we present our methodology by formally introducing the problem and describing our approach to leveraging DMs for image reconstruction.

4.1 Problem Definition

Threat Model. Our work builds upon an attack scenario on DP-SGD training, wherein an adversary can manipulate both the model and the loss function such that the input data is encoded into the gradient. Through the application of DP-SGD, the clipped and noisy gradient is equivalent to a scaled, noisy version of the target image (see [4, 56] for details). The adversary also possesses knowledge about the noise variance and some image prior. We note that for many real-world scenarios, the assumed capabilities can be mitigated by simple countermeasures. However, we consider it relevant as it represents one of the most threatening scenarios in real-world workflows, subsuming all weaker threat models.

Adversarial Problem Statement. Given a perturbed image \mathbf{x}_{priv} privatized by some DP-SGD algorithm, with parameters C and σ , i.e.,

$$\mathbf{x}_{\text{priv}} = \frac{1}{\lambda} \mathbf{x} + \boldsymbol{\xi}, \quad (7)$$

where $\lambda = \max(\|\mathbf{x}\|_2 / C, 1)$ denotes the linear factor from clipping, $\mathbf{x} \sim q(\mathbf{x})$ denotes the original image sampled from data distribution $q(\mathbf{x})$, and $\boldsymbol{\xi}$ is sampled from i.i.d. Gaussian noise $\mathcal{N}(\mathbf{0}, C^2 \sigma^2 \mathbf{I})$, the task is to reconstruct the private information in \mathbf{x} from \mathbf{x}_{priv} to assess the practical privacy leakage and the levels of sufficient noise perturbations.

Given that there is no clear way to generally define when private information is leaked, we define a *successful reconstruction attack* as achieving full reconstruction of the original image. Thus, we yield a denoising problem, requiring a denoiser $d : \mathbf{x}_{\text{priv}} \mapsto \mathbf{x}$ mapping the privatized image to the original image.

4.2 Private Image Reconstruction with DMs

DMs learn a strong image prior that closely approximates the underlying data distribution $q(\mathbf{x})$. This can be used for reconstructing lost information by combining image context with prior knowledge. Additionally, DMs have the ability to handle various levels of perturbations without the need for retraining. We leverage these inherent characteristics of DMs for our reconstruction attack.

Given the inverse problem in Eq. (7), we define the posterior over the observation as $q(\mathbf{x} | \mathbf{x}_{\text{priv}})$. We approximate this posterior using DMs and leverage their Markov chain to initiate the reverse process from a conditional intermediate state $p_\theta(\mathbf{x}_{t-1} | \mathbf{x}_{\text{priv}})$ instead of pure noise until the original image is recovered, i.e., $\mathbf{x}_0 \approx \mathbf{x}$. The easiest choice to integrate \mathbf{x}_{priv} into the reverse process is adopting the Variance Exploding (VE) form of DMs [43]:

$$\mathbf{x}_t = \mathbf{x}_0 + \sigma_t \boldsymbol{\epsilon}, \text{ with } \boldsymbol{\epsilon} \sim \mathcal{N}(\mathbf{0}, \mathbf{I}), \quad (8)$$

with variance schedule¹ $\{\sigma_t^2\}_{t=1}^T$ and $\sigma_T^2 \rightarrow \infty$. Notice that this formulation does not reduce the signal by $\sqrt{\bar{\alpha}_t}$, which is also the case in Eq. (7). However, the VE form complicates hyperparameter tuning since standard DMs employ the Variance Preserving (VP) form, where $\sqrt{1 - \bar{\alpha}_T} \rightarrow 1$ (see Eq. (5)). To utilize the VP form, we use the equivalence between the two forms [28] and define the starting point of the reverse process as follows:

$$\mathbf{x}_{t_{\text{start}}} = \frac{1}{\sqrt{1 + \sigma_{t_{\text{start}}}^2}} \mathbf{x}_{\text{priv}} = \frac{1}{\sqrt{1 + \sigma_{t_{\text{start}}}^2}} \left(\frac{1}{\lambda} \mathbf{x} + \boldsymbol{\xi} \right). \quad (9)$$

¹Note that σ_t denotes the noise variance relative to \mathbf{x}_0 , which differs from β_t and $\bar{\alpha}_t$ in the standard DM definition (see Sec. 3.2), as well as from σ in DP (see Sec. 3.1).

Handling the Clipping Factor λ . An unknown parameter in Eq. (9) is the linear scalar λ introduced by the clipping operation of DP-SGD. This parameter scales down the image, reducing its brightness and value range. In a realistic scenario, the exact value of λ is unknown to the adversary. However, given that λ represents a single value and images are typically characterized by a constrained range of color values, the adversary can easily approximate λ through normalization or trial-and-error (see Appendix A). Therefore, we assume the worst-case scenario, wherein the adversary successfully recovers the exact value of λ .

We stress that knowing λ comes with little advantage to the adversary, as it only enables them to rescale the image after perturbation, which increases the noise by factor λ (see Eq. (10)). Thus, the signal-to-noise ratio remains unchanged. Combining our assumption with Eq. (9) yields:

$$\mathbf{x}_{t_{\text{start}}} = \frac{\lambda}{\sqrt{1 + \sigma_{t_{\text{start}}}^2}} \mathbf{x}_{\text{priv}} = \frac{1}{\sqrt{1 + \sigma_{t_{\text{start}}}^2}} (\mathbf{x} + \lambda \boldsymbol{\xi}). \quad (10)$$

Markov Chain Matching. The Markov chain of (discrete) DMs is based on a pre-defined noise schedule $\{\beta_t\}_{t=1}^T$ and, therefore, does not contain a state for all possible noise variances. Thus, to initiate the reverse process from a perturbed image with variance $\hat{\sigma}^2 = C^2 \sigma^2 \lambda^2$, we must compute the variance schedule

$$\sigma_t = \sqrt{\frac{1}{\prod_{s=1}^t (1 - \beta_s)} - 1} = \sqrt{\frac{1}{\bar{\alpha}_t} - 1} \quad (11)$$

and search the next largest state t_{start} under the condition $\sigma_{t_{\text{start}}} > \hat{\sigma}$. The condition is required for adapting the noise variance by introducing additional noise, accounting for possibly large differences between σ_t and σ_{t-1} .

Enforcing Data Consistency. The stochastic generative process of DMs introduces randomness after each denoising step, increasing sample diversity (see Eq. (6)). However, this is not desirable in reconstruction problems, where the results should closely resemble the original. Therefore, we enforce data consistency by adopting the deterministic generation process of denoising diffusion implicit models (DDIMs) [41], which has been shown to retain image features throughout the generation process:

$$\mathbf{x}_{t-1} = \sqrt{\bar{\alpha}_{t-1}} \left(\frac{\mathbf{x}_t - \sqrt{1 - \bar{\alpha}_t} \cdot \boldsymbol{\epsilon}_\theta^{(t)}(\mathbf{x}_t)}{\sqrt{\bar{\alpha}_t}} \right) + \sqrt{1 - \bar{\alpha}_{t-1}} \cdot \boldsymbol{\epsilon}_\theta^{(t)}(\mathbf{x}_t). \quad (12)$$

Data consistency can also be enforced by conditioning every step of the reverse process on \mathbf{x}_{priv} by, *e.g.*, concatenating the low-quality sample to each latent state \mathbf{x}_t , yielding the posterior distribution $p_\theta(\mathbf{x}_{t-1} | \mathbf{x}_{\text{priv}}, \mathbf{x}_t)$. However, our scenario considers extreme cases where the images are heavily perturbed. Conditioning with such low-quality images causes harmful effects on the generation of DMs [30]. Thus, we forgo such an approach.

Algorithm 1 summarizes our method.

Alg. 1: Private Image Reconstruction with DMs

Require: $\mathbf{x}_{\text{priv}} = \lambda \mathbf{x} + \boldsymbol{\xi}$, with $\boldsymbol{\xi} \sim \mathcal{N}(0, C^2 \sigma^2 \mathbf{I})$, noise schedule $\bar{\alpha}_t$, model θ

- 1: $\sigma_t = \sqrt{\frac{1}{\bar{\alpha}_t} - 1}$
- 2: $\mathbf{x}'_{\text{priv}} = \lambda \mathbf{x}_{\text{priv}}$
- 3: $t_{\text{start}} = \arg \min_t (\sigma_t - C \sigma \lambda) \forall \sigma_t > C \sigma \lambda$
- 4: $\bar{\mathbf{x}}_{\text{priv}} = \mathbf{x}'_{\text{priv}} + \bar{\boldsymbol{\xi}}$, with $\bar{\boldsymbol{\xi}} \sim \mathcal{N}(\mathbf{0}, \sigma_{t_{\text{start}}}^2 - C^2 \sigma^2 \lambda^2 \mathbf{I})$
- 5: $\mathbf{x}_{t_{\text{start}}} = \frac{1}{\sqrt{1 + \sigma_{t_{\text{start}}}^2}} \bar{\mathbf{x}}_{\text{priv}}$
- 6: **for** $t = t_{\text{start}}, \dots, 1$ **do**
- 7: $\mathbf{x}_{t-1} = \sqrt{\bar{\alpha}_{t-1}} \left(\frac{\mathbf{x}_t - \sqrt{1 - \bar{\alpha}_t} \cdot \boldsymbol{\epsilon}_\theta^{(t)}(\mathbf{x}_t)}{\sqrt{\bar{\alpha}_t}} \right) + \sqrt{1 - \bar{\alpha}_{t-1}} \cdot \boldsymbol{\epsilon}_\theta^{(t)}(\mathbf{x}_t)$,
- 8: **end for**

5 Experiments

This section investigates the effectiveness of our reconstruction attack leveraging image priors learned by DMs and compares it to prevailing reconstruction bounds. For experimental details and ablation experiments, refer to Appendices B and C, respectively.

5.1 Experimental Setting

We use the Diffusers library [46] (based on PyTorch [34]) to leverage state-of-the-art pre-trained DMs for implementing our reconstruction attack. Our experimentation includes three datasets: CIFAR-10 [29], CelebA-HQ [27], and ImageNet-1K [11], with the latter two resized to 256×256 . For evaluation, we randomly select a subset of 5,000 test images from each dataset and quantitatively measure the reconstruction success with mean squared error (MSE), VGG-based learned perceptual image patch similarity (LPIPS) [40, 54], and structural similarity index measure (SSIM) [47].

We report results with respect to $\mu = C/\sigma$, where C denotes the clipping parameter and σ the noise multiplier of DP-SGD. It can be interpreted as a signal-to-noise ratio (SNR), where C bounds the signal and σ represents the noise. Analogously to the privacy parameter ϵ , a *lower* μ

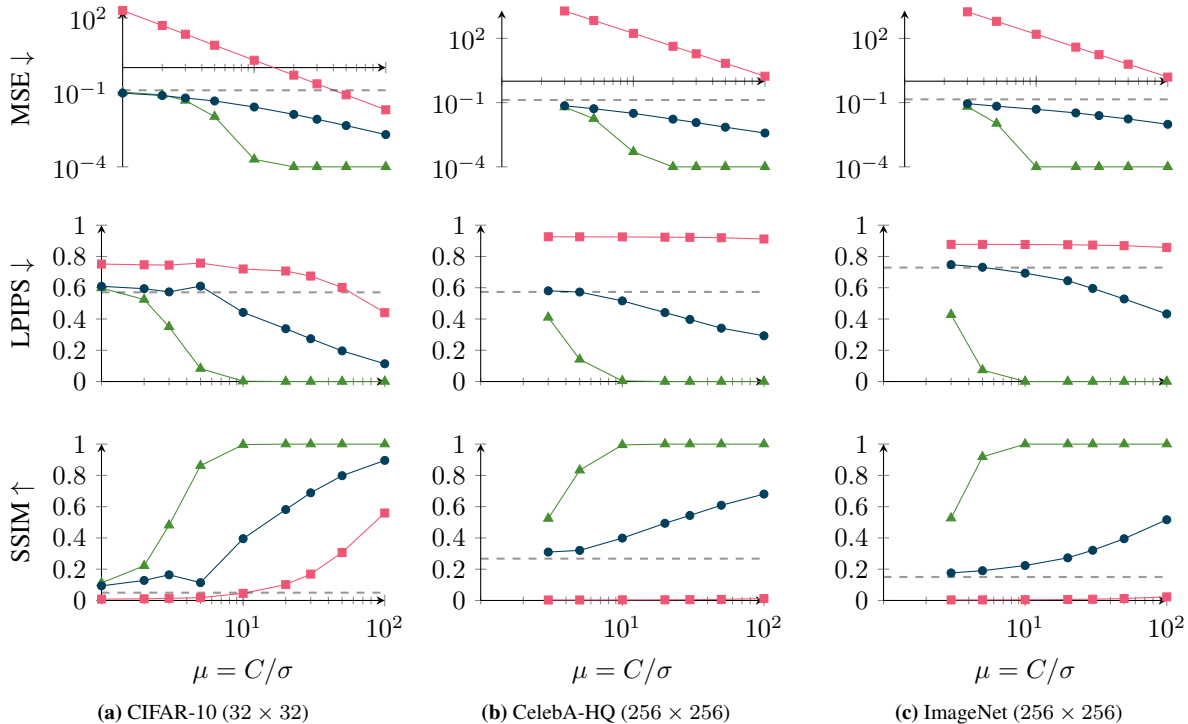


Fig. 2: Average similarity of image reconstructions. We compute the similarity between the original and the reconstructed images from our DM attack (blue \bullet), Ziller *et al.*'s attack [56] (red \blacksquare), and the ReRo attack [21] (green \blacktriangle). For $\mu < 3$, CelebA-HQ and ImageNet images exceed the maximal noise variance σ_T in the schedule; thus, no results can be given. The *dashed* line represents average similarity between test images, indicating at which point reconstructions become unrelated to the original.

(SNR) makes reconstruction more difficult and, thus, corresponds to a *higher* privacy guarantee. We note that given a specific setting, μ can be converted to the (ϵ, δ) notion.

5.2 Reconstruction Success under Different Data Priors

In this experiment, we assess the privacy leakage resulting from reconstruction attacks assuming different data priors. We compare the efficacy of our reconstruction attack, which leverages a realistic data prior, to the underlying attacks of the $(0, \gamma)$ -ReRo bound assuming access to the target image within a prior set of 256 images [21] and Ziller *et al.*'s bound [56] assuming no data access.

The results in Fig. 2 show that our reconstruction error is lower than the lower bound of an uninformed adversary but higher than the worst-case bound. As expected, the ReRo bound is overly pessimistic, assuming a powerful attack achieving mostly perfect similarity. Such an attack success is unrealistic, especially for the challenging ImageNet dataset. On the other side, as image size increases, the gap to Ziller *et al.*'s bound increases², revealing a sig-

nificant weakness of their method. Images with the same SNR exhibit similar reconstruction difficulty. Thus, image size should not significantly impact reconstruction success under the same μ . This is followed in DP and ReRo formulations, which use the SNR ratio C/σ , while Ziller *et al.*'s bounds depend on $C\sigma$, leading to error values which do not represent the actual difficulty of reconstruction.

Regarding our reconstruction success, a “phase transition” becomes apparent. For $\mu \leq 5$, the similarity of our reconstructions to the original converges to the average similarity of test images (dashed line in Fig. 2), suggesting that these are random generations instead of reconstructions of the original image. This is because DMs always generate samples from the underlying data distribution, which inherently will be closer to the original than the perturbed image.

We present qualitative results in Fig. 3 and Appendix D, confirming the effectiveness of our attack. Here, we observe an additional phase transition at $\mu = 20$, where reconstructed images start deviating from the original while still sharing similar high-level attributes such as dataset class, image color, or gender. Additionally, as observed in Fig. 2, for $\mu \leq 5$, the reconstructions become unrelated to the original, indicating good privacy protection.

²Notice that in Fig. 2, LPIPS and SSIM for Ziller *et al.*'s attack always converge, while the MSE does not. This is due to the clipping of color values between 0 and 1 required for computing LPIPS and SSIM.

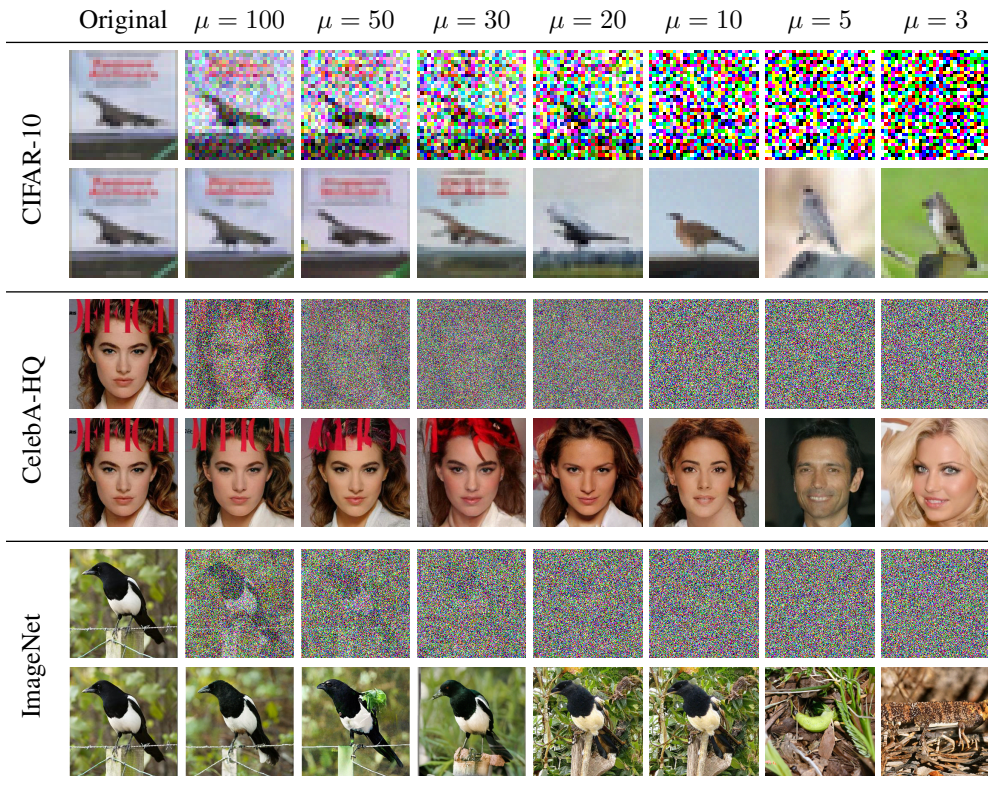


Fig. 3: Reconstruction results with respect to $\mu = C/\sigma$. For each dataset, the reconstructed image from Ziller *et al.*'s attack (*top*) and our DM attack (*bottom*) are shown. The top images also represent the input of our attack.

5.3 Reconstruction Success under Distribution Shift

Previously, we assumed the adversary has access to training data with the same underlying data distribution as the target (test) data, which enables them to learn a strong data prior. In the next experiment, we investigate three scenarios where the data prior does not stem from the same distribution, *i.e.*, an out-of-distribution prior, which is weaker than in-distribution priors. We perform this experiment in three settings: (1) The DM is trained on CIFAR-10 and is used to reconstruct test images from CIFAR-100 [29]. These datasets are very similar, differing primarily in class number and diversity. (2) An ImageNet DM reconstructs CelebA-HQ face images, and (3) the same DM reconstructs grayscale chest X-ray images from the CheXpert dataset [24]. Intuitively, the greater the discrepancy between training and test data, the larger the distribution shift.

The results in Figs. 4 and 5 show a clear trend: larger distribution shifts (weaker data priors) lead to decreased reconstruction success. This is particularly evident from the shift in the privacy guarantee (μ -value) at which the similarity of the reconstructions surpasses the average similarity of the test datasets (dashed line in Fig. 4). Irrespective of the error function, it is a good indicator for less-than-useful reconstructions, which are more similar to the

training data than the target images.

Our findings demonstrate the significant impact of data distribution shift on the reconstruction performance of DMs, especially in high privacy regimes. However, our method yields reasonable reconstructions for low privacy guarantees even in scenarios with significant distribution shifts.

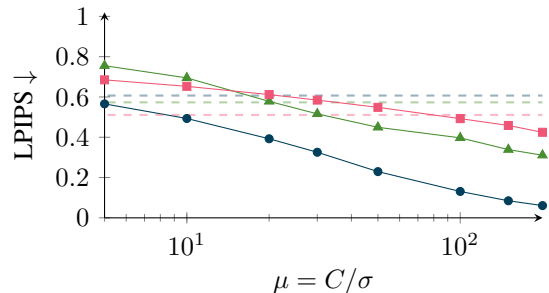


Fig. 4: Reconstruction success under distribution shift. The performance of the DM trained on CIFAR-10 and tested on CIFAR-100 (blue ●), and the ImageNet DM tested on CelebA-HQ (green ▲) and CheXpert (red ■) are shown. The dashed line represents average similarity between test images of the datasets (same color). The results show the significant influence of distribution shift between the data prior and the reconstruction target.

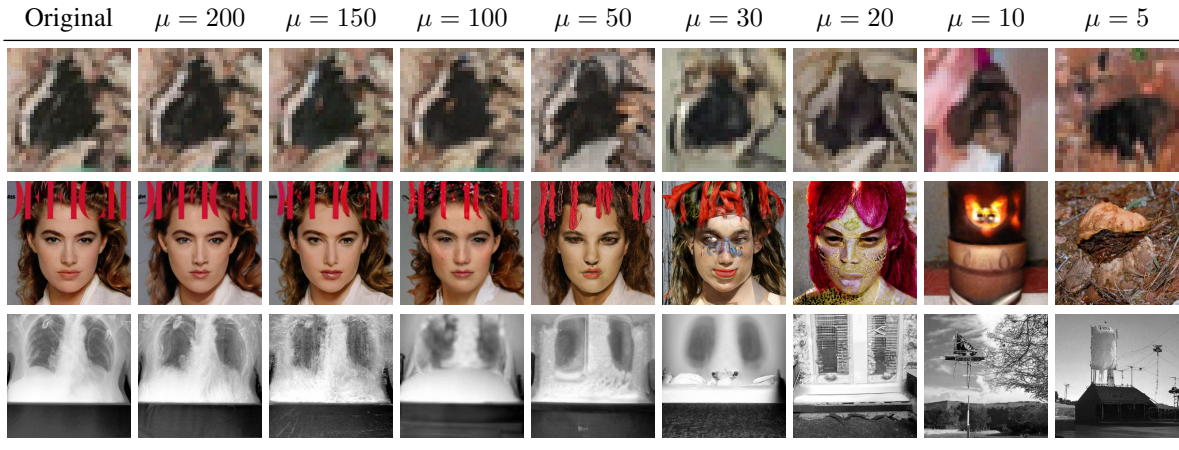


Fig. 5: Reconstruction results under distribution shift. The performance of the DM trained on CIFAR-10 and tested on CIFAR-100 (*top*), and the performance of the ImageNet DM on CelebA-HQ (*middle*) and CheXpert (*bottom*) are shown.

5.4 Estimating Reconstruction Success without Target Access

DMs always generate a candidate reconstruction, even when the perturbed image lacks any information for reconstruction. This implies that the resulting reconstructions may differ from the target images. While this is useful for data owners and practitioners who can directly compare the features of the reconstructions with the original images, adversaries lacking access to the original image (reconstruction target) may struggle to infer which features are made up by the DM. However, we propose that adversaries can overcome this challenge by generating multiple candidate reconstructions using the probabilistic generation process of, *e.g.*, DDPMs (see Eq. (6)) and assess which features stay consistent across reconstructions. Such features are most likely to originate from the reconstruction target. This is analog to a *maximum a posteriori* attack, where the mode of the empirically generated images is computed.

Fig. 6 shows the average pairwise similarity between five DDPM generations from each of the 5,000 noisy images under different privacy levels, providing insights into estimating the reconstruction success using such an approach. It shows that, for all datasets, the true reconstruction success (dashed lines in Fig. 6) can be estimated well without access to the original image. We provide qualitative results in Supplementary Fig. 13, which demonstrates the shared features among different generations. In our example, gender can be inferred until $\mu = 5$, and the hair color remains consistent until $\mu = 20$.

These findings highlight that visual insights from DMs’ reconstructions hold value not only for data owners comparing reconstructions with the original images, but also for adversaries who only have access to the noisy image and multiple generations.

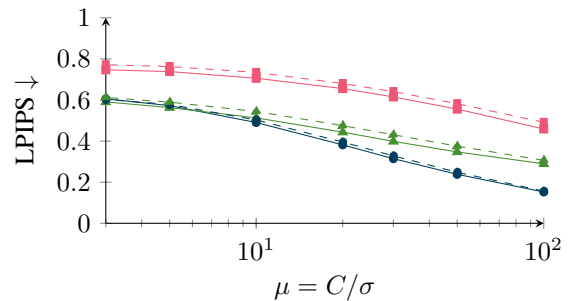


Fig. 6: Reconstruction success estimated from average similarity between multiple DDPM samples of CIFAR-10 (blue ●), CelebA (green ▲), and ImageNet (red ■) compared to the true success obtained by computing the average similarity between reconstructions and the original images (dashed line). The closeness between same colored lines shows that the original image is not required to estimate the reconstruction success well.

6 Discussion and Conclusion

This work investigates the effect of real-world data priors on the success of data reconstruction attacks, revealing a discrepancy between existing theoretical models of reconstruction bounds and the outcome of practical attacks. Our findings indicate that the strength of the data prior significantly influences the reconstruction success, positioning our attack between the $(0, \gamma)$ -ReRo bound and Ziller *et al.*’s bound. This underscores the difficulty and necessity of accurately incorporating data priors into formal privacy guarantees on data reconstruction success, ensuring better alignment with real-world scenarios. However, we acknowledge that in domains where acquiring accurate data priors is challenging, threat models assuming no data prior, such as the threat model proposed by Ziller *et al.*, remain relevant and realistic. We also recognize the flexibility

of the ReRo bound with respect to incorporating different data priors. Nevertheless, addressing challenges related to defining appropriate prior knowledge and error functions will be paramount for its effective implementation.

Furthermore, we find that strong image priors parameterized by DMs exhibit remarkable success in extracting information from heavily perturbed images, surpassing human visual capabilities. Additionally, our method significantly improves the reconstruction outcomes of previous methods [4, 56] through a simple post-processing step. Given the widespread availability of DMs for various data distributions, it is reasonable to assume that adversaries can profit from their capabilities. The simplicity and accessibility of our method broaden the scope of potential adversaries who could utilize such techniques, increasing the urgency for robust defenses to counter such threats.

We propose DMs as a method for visual auditing of privacy settings. Specifically, our reconstructions effectively capture the residual information within perturbed images, providing valuable insights for practitioners of DP. Unlike formal privacy parameters, which are challenging to interpret for non-experts [9], DMs offer tangible means of visualizing privacy leakage, thereby facilitating communication with stakeholders and enhancing their comprehension of privacy guarantees. For instance, when a DM generates an image from the same class but with different low-level features compared to the original, it suggests that low-level features are privatized, whereas the class information can be disclosed. Consequently, DMs can serve as effective visual auditing tools for evaluating the kind and quantity of information that can be extracted under various privacy guarantees and support the selection and understanding of privacy parameters.

We note that our work is limited to a specific threat model and attack scenario, assuming that the adversary has access to intermediate training gradients and has the capability to manipulate the network architecture and loss function. Such capabilities and attacks may be relevant to settings like federated learning (FL) with malicious servers. However, even in FL, simple countermeasures often suffice to prevent such modifications. Consequently, our analysis may show higher reconstruction success than what would be achievable in many real-world settings. However, by this, we ensure that our findings provide a good indication of the maximum currently feasible reconstruction success. Hence, an interesting direction for future work would be to investigate the reconstruction success under additional threat models.

In summary, our work contributes to the development of techniques which can assist stakeholders, including those with no formal mathematical background, in interpreting the implications of adversarial interference and its mitigation through privacy-enhancing techniques like DP.

Impact Statement

This work proposes a data reconstruction attack capable of disclosing sensitive information from real-world ML models. While our method can be used maliciously, we use it to highlight how to defend against data reconstruction attacks using privacy methods like DP and how our attack can be utilized as a tool for non-experts to select sufficient privacy guarantees. Furthermore, we only utilize publicly available images, thereby not exposing data that is not already available.

Acknowledgement

We thank Jonas Kuntzer for proofreading the article.

References

- [1] M. Abadi, A. Chu, I. Goodfellow, H. B. McMahan, I. Mironov, K. Talwar, and L. Zhang. Deep learning with differential privacy. In *Proceedings of the 2016 ACM SIGSAC Conference on Computer and Communications Security, CCS '16*, page 308–318, New York, NY, USA, 2016. Association for Computing Machinery.
- [2] B. Balle, G. Cherubin, and J. Hayes. Reconstructing training data with informed adversaries. In *2022 IEEE Symposium on Security and Privacy (SP)*, pages 1138–1156. IEEE Computer Society, 2022.
- [3] B. Balle and Y.-X. Wang. Improving the gaussian mechanism for differential privacy: Analytical calibration and optimal denoising. In *International Conference on Machine Learning*, 2018.
- [4] F. Boenisch, A. Dziedzic, R. Schuster, A. S. Shamsabadi, I. Shumailov, and N. Papernot. Reconstructing individual data points in federated learning hardened with differential privacy and secure aggregation. In *2023 IEEE 8th European Symposium on Security and Privacy (EuroS&P)*, pages 241–257, 2023.
- [5] F. Boenisch, A. Dziedzic, R. Schuster, A. S. Shamsabadi, I. Shumailov, and N. Papernot. When the curious abandon honesty: Federated learning is not private. In *2023 IEEE 8th European Symposium on Security and Privacy (EuroS&P)*, pages 175–199, Los Alamitos, CA, USA, jul 2023. IEEE Computer Society.
- [6] N. Carlini, J. Hayes, M. Nasr, M. Jagielski, V. Shwag, F. Tramèr, B. Balle, D. Ippolito, and E. Wallace. Extracting training data from diffusion models. In *Proceedings of the 32nd USENIX Conference on*

- Security Symposium, SEC '23, USA, 2023. USENIX Association.*
- [7] S. Chang, B. Yu, and M. Vetterli. Adaptive wavelet thresholding for image denoising and compression. *IEEE Transactions on Image Processing*, 9(9):1532–1546, 2000.
- [8] H. Chung, E. S. Lee, and J. C. Ye. Mr image denoising and super-resolution using regularized reverse diffusion. *IEEE Transactions on Medical Imaging*, 42(4):922–934, 2023.
- [9] R. Cummings, D. Desfontaines, D. Evans, R. Geambasu, Y. Huang, M. Jagielski, P. Kairouz, G. Kamath, S. Oh, O. Ohrimenko, N. Papernot, R. Rogers, M. Shen, S. Song, W. Su, A. Terzis, A. Thakurta, S. Vassilvitskii, Y.-X. Wang, L. Xiong, S. Yekhanin, D. Yu, H. Zhang, and W. Zhang. Advancing Differential Privacy: Where We Are Now and Future Directions for Real-World Deployment. *Harvard Data Science Review*, jan 16 2024. <https://hdr.mitpress.mit.edu/pub/sl9we8gh>.
- [10] K. Dabov, A. Foi, V. Katkovnik, and K. Egiazarian. Image denoising by sparse 3-d transform-domain collaborative filtering. *IEEE Transactions on Image Processing*, 16(8):2080–2095, 2007.
- [11] J. Deng, W. Dong, R. Socher, L.-J. Li, K. Li, and L. Fei-Fei. Imagenet: A large-scale hierarchical image database. In *2009 IEEE Conference on Computer Vision and Pattern Recognition*, pages 248–255, 2009.
- [12] P. Dhariwal and A. Q. Nichol. Diffusion models beat GANs on image synthesis. In A. Beygelzimer, Y. Dauphin, P. Liang, and J. W. Vaughan, editors, *Advances in Neural Information Processing Systems*, 2021.
- [13] J. Dong, A. Roth, and W. J. Su. Gaussian Differential Privacy. *Journal of the Royal Statistical Society Series B: Statistical Methodology*, 84(1):3–37, 02 2022.
- [14] D. L. Donoho and I. M. Johnstone. Ideal spatial adaptation by wavelet shrinkage. *Biometrika*, 81(3):425–455, 09 1994.
- [15] C. Dwork and A. Roth. The algorithmic foundations of differential privacy. *Found. Trends Theor. Comput. Sci.*, 9(3–4):211–407, aug 2014.
- [16] M. Elad, B. Kawar, and G. Vaksman. Image denoising: The deep learning revolution and beyond—a survey paper. *SIAM Journal on Imaging Sciences*, 16(3):1594–1654, 2023.
- [17] L. H. Fowl, J. Geiping, W. Czaja, M. Goldblum, and T. Goldstein. Robbing the fed: Directly obtaining private data in federated learning with modified models. In *International Conference on Learning Representations*, 2022.
- [18] J. Geiping, H. Bauermeister, H. Dröge, and M. Moeller. Inverting gradients - how easy is it to break privacy in federated learning? In H. Larochelle, M. Ranzato, R. Hadsell, M. Balcan, and H. Lin, editors, *Advances in Neural Information Processing Systems*, volume 33, pages 16937–16947. Curran Associates, Inc., 2020.
- [19] C. Guo, B. Karrer, K. Chaudhuri, and L. van der Maaten. Bounding training data reconstruction in private (deep) learning. In K. Chaudhuri, S. Jegelka, L. Song, C. Szepesvari, G. Niu, and S. Sabato, editors, *Proceedings of the 39th International Conference on Machine Learning*, volume 162 of *Proceedings of Machine Learning Research*, pages 8056–8071. PMLR, 17–23 Jul 2022.
- [20] N. Haim, G. Vardi, G. Yehudai, O. Shamir, and M. Irani. Reconstructing training data from trained neural networks. In S. Koyejo, S. Mohamed, A. Agarwal, D. Belgrave, K. Cho, and A. Oh, editors, *Advances in Neural Information Processing Systems*, volume 35, pages 22911–22924. Curran Associates, Inc., 2022.
- [21] J. Hayes, B. Balle, and S. Mahloujifar. Bounding training data reconstruction in DP-SGD. In *Thirty-seventh Conference on Neural Information Processing Systems*, 2023.
- [22] M. Heusel, H. Ramsauer, T. Unterthiner, B. Nessler, and S. Hochreiter. Gans trained by a two time-scale update rule converge to a local nash equilibrium. In *Proceedings of the 31st International Conference on Neural Information Processing Systems, NIPS'17*, page 6629–6640, Red Hook, NY, USA, 2017. Curran Associates Inc.
- [23] J. Ho, A. Jain, and P. Abbeel. Denoising diffusion probabilistic models. In *Proceedings of the 34th International Conference on Neural Information Processing Systems, NIPS'20*, Red Hook, NY, USA, 2020. Curran Associates Inc.
- [24] J. Irvin, P. Rajpurkar, M. Ko, Y. Yu, S. Ciurea-Ilcus, C. Chute, H. Marklund, B. Haghgoo, R. Ball, K. Shpanskaya, J. Seekins, D. A. Mong, S. S. Halabi, J. K. Sandberg, R. Jones, D. B. Larson, C. P. Langlotz, B. N. Patel, M. P. Lungren, and A. Y. Ng. Chexpert: A large chest radiograph dataset with uncertainty labels and expert comparison. *Proceedings*

- of the AAAI Conference on Artificial Intelligence, 33(01):590–597, Jul. 2019.
- [25] G. Kaissis, J. Hayes, A. Ziller, and D. Rueckert. Bounding data reconstruction attacks with the hypothesis testing interpretation of differential privacy, 2023.
- [26] G. Kaissis, A. Ziller, S. Kolek, A. Riess, and D. Rueckert. Optimal privacy guarantees for a relaxed threat model: Addressing sub-optimal adversaries in differentially private machine learning. In *Thirty-seventh Conference on Neural Information Processing Systems*, 2023.
- [27] T. Karras, T. Aila, S. Laine, and J. Lehtinen. Progressive growing of GANs for improved quality, stability, and variation. In *International Conference on Learning Representations*, 2018.
- [28] B. Kawar, M. Elad, S. Ermon, and J. Song. Denoising diffusion restoration models. In A. H. Oh, A. Agarwal, D. Belgrave, and K. Cho, editors, *Advances in Neural Information Processing Systems*, 2022.
- [29] A. Krizhevsky and G. Hinton. Learning multiple layers of features from tiny images. Technical Report 0, University of Toronto, Toronto, Ontario, 2009.
- [30] X. Li, Y. Ren, X. Jin, C. Lan, X. Wang, W. Zeng, X. Wang, and Z. Chen. Diffusion models for image restoration and enhancement – a comprehensive survey, 2023.
- [31] J. Lokna, A. Paradis, D. I. Dimitrov, and M. Vechev. Group and attack: Auditing differential privacy. In *Proceedings of the 2023 ACM SIGSAC Conference on Computer and Communications Security*, 2023.
- [32] M. Nasr, J. Hayes, T. Steinke, B. Balle, F. Tramèr, M. Jagielski, N. Carlini, and A. Terzis. Tight auditing of differentially private machine learning. In *Proceedings of the 32nd USENIX Conference on Security Symposium, SEC '23, USA, 2023*. USENIX Association.
- [33] M. Nasr, S. Song, A. Thakurta, N. Papernot, and N. Carlini. Adversary instantiation: Lower bounds for differentially private machine learning. In *2021 IEEE Symposium on Security and Privacy (SP)*, pages 866–882. IEEE Computer Society, 2021.
- [34] A. Paszke, S. Gross, F. Massa, A. Lerer, J. Bradbury, G. Chanan, T. Killeen, Z. Lin, N. Gimeshein, L. Antiga, A. Desmaison, A. Köpf, E. Yang, Z. DeVito, M. Raison, A. Tejani, S. Chilamkurthy, B. Steiner, L. Fang, J. Bai, and S. Chintala. *PyTorch: an imperative style, high-performance deep learning library*. Curran Associates Inc., Red Hook, NY, USA, 2019.
- [35] N. Pearl, Y. Brodsky, D. Berman, A. Zomet, A. R. Acha, D. Cohen-Or, and D. Lischinski. Svr: Spatially-variant noise removal with denoising diffusion, 2023.
- [36] N. Ponomareva, H. Hazimeh, A. Kurakin, Z. Xu, C. Denison, H. B. McMahan, S. Vassilvitskii, S. Chien, and A. G. Thakurta. How to dp-fy ml: A practical guide to machine learning with differential privacy. *Journal of Artificial Intelligence Research*, 77:1113–1201, July 2023.
- [37] J. L. Rodgers and W. A. Nicewander. Thirteen ways to look at the correlation coefficient. *The American Statistician*, 42(1):59–66, 1988.
- [38] O. Ronneberger, P. Fischer, and T. Brox. U-net: Convolutional networks for biomedical image segmentation. In N. Navab, J. Hornegger, W. M. Wells, and A. F. Frangi, editors, *Medical Image Computing and Computer-Assisted Intervention – MICCAI 2015*, pages 234–241, Cham, 2015. Springer International Publishing.
- [39] T. Salimans, A. Karpathy, X. Chen, and D. P. Kingma. PixelCNN++: Improving the pixelCNN with discretized logistic mixture likelihood and other modifications. In *International Conference on Learning Representations*, 2017.
- [40] K. Simonyan and A. Zisserman. Very deep convolutional networks for large-scale image recognition. In *International Conference on Learning Representations*, 2015.
- [41] J. Song, C. Meng, and S. Ermon. Denoising diffusion implicit models. In *International Conference on Learning Representations*, 2021.
- [42] S. Song, K. Chaudhuri, and A. D. Sarwate. Stochastic gradient descent with differentially private updates. In *2013 IEEE Global Conference on Signal and Information Processing*, pages 245–248, 2013.
- [43] Y. Song, J. Sohl-Dickstein, D. P. Kingma, A. Kumar, S. Ermon, and B. Poole. Score-based generative modeling through stochastic differential equations. In *International Conference on Learning Representations*, 2021.
- [44] T. Steinke, M. Nasr, and M. Jagielski. Privacy auditing with one (1) training run. In *Thirty-seventh Conference on Neural Information Processing Systems*, 2023.

- [45] S. van der Walt, J. L. Schönberger, J. Nunez-Iglesias, F. Boulogne, J. D. Warner, N. Yager, E. Gouillart, T. Yu, and the scikit-image contributors. scikit-image: image processing in Python. *PeerJ*, 2:e453, 6 2014.
- [46] P. von Platen, S. Patil, A. Lozhkov, P. Cuenca, N. Lambert, K. Rasul, M. Davaadorj, and T. Wolf. Diffusers: State-of-the-art diffusion models. <https://github.com/huggingface/diffusers>, 2022.
- [47] Z. Wang, A. Bovik, H. Sheikh, and E. Simoncelli. Image quality assessment: from error visibility to structural similarity. *IEEE Transactions on Image Processing*, 13(4):600–612, 2004.
- [48] T. Xiang, W. Yue, Y. Lin, J. Yang, Z. Wang, and X. Li. Diffcmr: Fast cardiac mri reconstruction with diffusion probabilistic models, 2023.
- [49] T. Xiang, M. Yurt, A. B. Syed, K. Setsompop, and A. Chaudhari. DDMS²: Self-supervised diffusion MRI denoising with generative diffusion models. In *The Eleventh International Conference on Learning Representations*, 2023.
- [50] Y. Xie, M. Yuan, B. Dong, and Q. Li. Diffusion model for generative image denoising, 2023.
- [51] C. Yang, L. Liang, and Z. Su. Real-world denoising via diffusion model, 2023.
- [52] S. Yeom, I. Giacomelli, M. Fredrikson, and S. Jha. Privacy risk in machine learning: Analyzing the connection to overfitting. In *2018 IEEE 31st Computer Security Foundations Symposium (CSF)*, pages 268–282, 2018.
- [53] H. Zhang, J. Hong, Y. Deng, M. Mahdavi, and J. Zhou. Understanding deep gradient leakage via inversion influence functions. In *Thirty-seventh Conference on Neural Information Processing Systems*, 2023.
- [54] R. Zhang, P. Isola, A. A. Efros, E. Shechtman, and O. Wang. The unreasonable effectiveness of deep features as a perceptual metric. In *2018 IEEE/CVF Conference on Computer Vision and Pattern Recognition (CVPR)*, pages 586–595, Los Alamitos, CA, USA, jun 2018. IEEE Computer Society.
- [55] A. Ziller, T. T. Mueller, S. Stieger, L. Feiner, J. Brandt, R. Braren, D. Rueckert, and G. Kaissis. Reconciling ai performance and data reconstruction resilience for medical imaging, 2023.
- [56] A. Ziller, A. Riess, K. Schwethelm, T. T. Mueller, D. Rueckert, and G. Kaissis. Bounding reconstruction attack success of adversaries without data priors, 2024.

A Approximating the Clipping Factor λ

Recall our assumption that the adversary has knowledge about the exact value of the clipping factor $\lambda = \max(\|\mathbf{x}\|_2/C, 1)$ in Eq. (7). In this section, we demonstrate the simplicity of yielding a good approximation of λ using trial-and-error.

As an example, we take an image from the CIFAR-10 dataset [29] and assume $C = 1$ (a standard value in DP-SGD practice [36]) and $\mu = C/\sigma = 30$. The example image has a L_2 -norm of $\|\mathbf{x}\|_2 = 27.24$, thus, it will be clipped and $\lambda = \|\mathbf{x}\|_2/C = 27.24$.

The first step of an adversary could be to set a value range for λ . Given the standard range of color values $x_i \in [0, 1]$, the maximum L_2 -norm of a flattened image $\mathbf{x} \in \mathbb{R}^{HWD}$ is \sqrt{HWD} , in this case, $(\|\mathbf{x}\|_2)_{\max} = \sqrt{32 \cdot 32 \cdot 3} = 55.43$ and, therefore, $\lambda \in [1, 55.43]$. Now, without further assumptions, the adversary can repeat the reconstruction process with different values for λ and select the best result. Fig. 7 shows some example results of the trial-and-error approach.

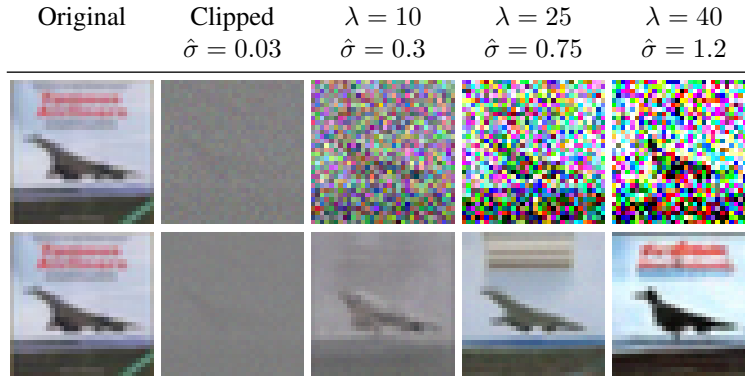


Fig. 7: Reconstruction results for different approximations of λ . The (scaled) perturbed image (*top*) and the DM’s reconstruction (*bottom*) are shown. Additionally, the change in the standard deviation of the noise $\hat{\sigma} = C\sigma\lambda$ resulting from rescaling is given.

B Experimental Details

Models. For the CIFAR-10 and CelebA-HQ datasets, we utilize the DMs and exponential moving average (EMA) checkpoints from Ho *et al.* [23]. These checkpoints achieve a validation Fréchet Inception Distance (FID) [22] of 3.17 for CIFAR-10, the FID for CelebA-HQ was not reported. For the ImageNet dataset, we employ the unconditional DM of Dhariwal and Nichol [12], which achieves a validation FID of 12.00. All DMs are based on U-Net architectures [38] and PixelCNN++ [39].

Compute Reconstruction Performance. To evaluate the reconstruction performance of the considered attacks, we assess the average similarity between the reconstructed test images and their original counterparts. First, we execute the reconstruction attack proposed by Ziller *et al.* [56] on DP-SGD (as described in Sec. 3), obtaining their reconstruction performance. Then, we post-process the noisy images generated by Ziller *et al.*’s attack using our proposed DM method (as described in Sec. 4), representing our attack’s reconstruction performance.

For the ReRo lower bound, we implement the prior-aware attack proposed by Hayes *et al.* [21] under identical DP-SGD settings and architectures as Ziller *et al.* [56]. We compute reconstructions by matching the noisy and clipped gradients from DP-SGD with the clipped gradients derived from a prior set comprising 256 candidate images using the dot product. The resulting matched images are then considered as reconstructions and used to compute the similarity. Intuitively, successful matching by the ReRo attack results in perfect reconstructions.

C Ablation Experiments

In this section, we conduct a series of ablation experiments to assess the performance of our reconstruction attack under different settings and assumptions. Each ablation experiment evaluates the average similarity between the reconstructed images and the original images using CIFAR-10 and LPIPS. In all figures, the dashed line represents the average similarity of test images.

Privacy Leakage from Re-Identification. In this experiment, we evaluate the capabilities of an adversary using our method for re-identification. For this, we employ the matching strategy introduced by Hayes *et al.* [21] (see Sec. 3.1) and match the reconstructed image with the most similar image from a prior set using LPIPS and compute the ratio of correct matches. We compare our matching success with the $(0, \gamma)$ -ReRo bound.

The results in Fig. 8 corroborate our expectation that our method achieves lower matching success than the ReRo bound. This difference can be attributed to our attack solely assuming a general data prior, while ReRo assumes access to the full underlying dataset. Consequently, our method relies on the DM-based reconstruction of the image, which may drop some information in the generation process. However, despite this limitation, our matching performance is notably close to the ReRo bound, indicating our attack’s ability to recover unique features even under strong perturbations. Once again, we observe that $\mu \leq 5$ serves as a threshold beyond which our attack cannot recover any unique features.

Comparison between DDIM and DDPM Generation. Recall that we employ the deterministic generation process of DDIMs to enforce data consistency. In this experiment, we evaluate the effect of this design choice on reconstruction performance by comparing DDIM generation (see Eq. (12)) with the probabilistic generation process of DDPMs (see Eq. (6)), which is usually used in implementations of DMs.

The results in Fig. 9 show improved performance across various privacy levels with DDIM sampling, suggesting that DDIMs exhibit greater consistency and remain closer to the original image throughout the generation process.

Unknown Noise Variance. In our main experiments, we assume that the adversary knows the variance of the noise in the privatized image. However, this assumption may not always hold true in practical scenarios. In this experiment, we assess the impact of unknown noise variance on our reconstruction performance. For this, we approximate the noise variance using the wavelet-based implementation in `scikit-image` [45] (`restoration.estimate_sigma`), which is described in Section 4.2 of [14].

The results in Fig. 10 show only a slight decrease in reconstruction performance, indicating that the noise variance can be accurately estimated and that our attack is robust against estimation errors.

Denosing without Learned Data Priors. In this experiment, we assess the effectiveness of structural image priors that only capture patterns inherent in images, and do not approximate a specific data distribution. For this, we employ traditional denoising methods based on wavelet transformation [7] and BM3D [10] and compare their performance with our DM method approximating the underlying data distribution.

The results in Fig. 11 show the limitations of traditional denoising methods when confronted with large noise perturbations. Specifically, the results reveal a large performance difference across all privacy levels.

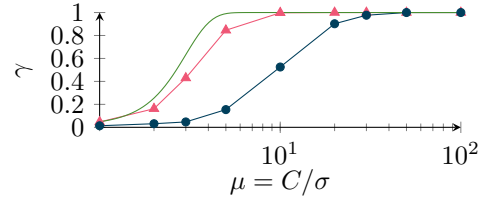


Fig. 8: Image matching success γ , with prior size of 256 using our reconstructed images (blue ●) compared to the ReRo lower (red ▲), and upper bound (green).

However, despite this limitation, our matching performance is notably close to the ReRo bound, indicating our attack’s ability to recover unique features even under strong perturbations. Once again, we observe that $\mu \leq 5$ serves as a threshold beyond which our attack cannot recover any unique features.

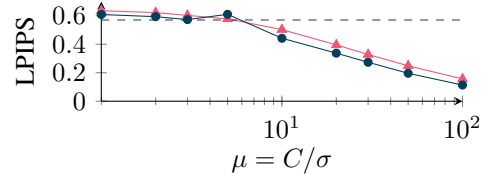


Fig. 9: DDIM (blue ●) and DDPM (red ▲) generation performance.

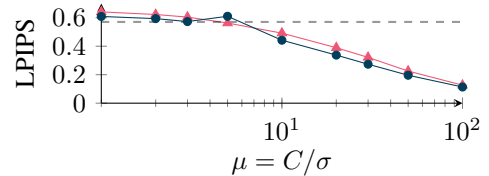


Fig. 10: Performance under known noise variance (blue ●) and noise variance estimation (red ▲).

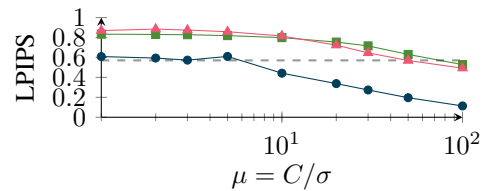


Fig. 11: Performance of traditional denoising methods based on wavelet transformation (green ■) and BM3D (red ▲) compared to our DM method (blue ●).

D Additional Reconstruction Results



Fig. 12: Reconstruction results of our DM attack with respect to $\mu = C/\sigma$ for CIFAR-10 (*top*), CelebA-HQ (*middle*), and ImageNet (*bottom*).



Fig. 13: DDPM reconstruction results with respect to $\mu = C/\sigma$ for a CelebA-HQ image. For each μ -value, the original image, the noisy image, and five reconstructions from the noisy image are shown. We observe that lower μ (SNR) lead to larger deviations between generations. The adversary is interested in the features that stay consistent across generations, as these likely originate from the original image. For example, hair color stays consistent until $\mu = 20$, and gender can be inferred until $\mu = 5$. This shows that the visual insights from reconstructions of DMs are not only valuable for data owners who can compare the reconstruction with the original image, but also for adversaries who only have access to the noisy image and the ability to compare different generations.